Innovative Infrastructure Solutions (2023) 8:50
https://doi.org/10.1007/s41062-022-01017-1

TECHNICAL PAPER

Experimental modeling of a single pile in liquefiable soil under the effect of coupled static-dynamic loads

Rusal S. Hussien[1] · **Bushra S. Albusoda**[2]

Received: 3 June 2022 / Accepted: 9 December 2022 / Published online: 23 December 2022

Abstract
In this work, a single pile is physically modeled and embedded in an upper liquefiable loose sand layer overlying a non-liquefiable dense layer. A laminar soil container is adopted to simulate the coupled static-dynamic loading pile response during earthquake motions: Ali Algharbi, Halabjah, El-Centro, and Kobe earthquakes. During seismic events with combined loading, the rotation along the pile, the lateral and vertical displacements at the pile head as well as the pore pressure ratio in loose sandy soil were assessed. According to the experimental findings, combined loading that ranged from 50 to 100% of axial load would alter the pile reaction by reducing the pile head peak ground acceleration, rotation of the pile, and lateral displacement for all input motions, while vertical displacement stabilizes as combined loading rises. In contrast, independent of the magnitude of the earthquake and soil depth, the impact of increasing the combined axial and lateral loading from 50 to 100% is limited. Due to the lateral loading's ability to greatly reduce acceleration, rotation, and lateral displacement at moderate earthquake motion, the pile cap was significantly restricted. When earthquake motion increases to a strong activity, it has a minimal impact. Since pore pressure is produced more quickly during a large earthquake than it is during a weak one, the magnitude and length of the earthquake have a significant impact on how much pore pressure is produced. The combined loading has only a small impact.

Keywords Pile in liquefiable soil · Shaking table test · Physical modeling · Coupled static-dynamic loading

Introduction

One of the most serious natural disasters that threaten humans and property, happened within a period of time, leaving catastrophic damage and losses in life of humans and buildings, bridges, dams, etc. These effects coming not only from strong earthquake motions but also from the deformation of the ground as a result of liquefaction. The term Liquefaction always referred to the behavior of saturated soil subjected to dynamic shear stress, coupled with a rapid decrease in volumetric strain, [1]. Due to the recent challenge and increase in the higher building that has been constructed in an area prone to seismic hazards and weak soil layer. A deep pile foundation manifests as a primary concern in solving this challenge. In this way, it could be subjected to a more complex situation like laterally cycling loads imposed from seismic, or it may face a loss in its tied properties during the liquefaction of soil or any other geological or constructed event. Arise from this problem; by using a more advanced testing technique in order to evaluate the pile foundation under different conditions to simulate the real fact the shaking soil table is one of these solutions. One of the significant effects on pile response in a seismically prone area is the (liquefaction of soil). Hence, the pile could behave in a complex manner due to the increasing buildup of excess pore pressure leading to soft saturated soil and consequently affecting the pile in terms of large bending moment and shear [2]. The collapse damage results from liquefaction are observed in pile foundations during and after strong earthquake events, despite the higher factor of safety implemented [3]. Different modes of pile foundation failure characteristics occurred during earthquake motion of liquefiable soil that concludes large settlement and progressive pore pressure. These characteristics are studied by

✉ Bushra S. Albusoda
dr.bushra_albusoda@coeng.uobaghdad.edu.iq

Rusal S. Hussien
salamrusal@gmail.com

[1] Al-Farabi University College, Baghdad, Iraq

[2] University of Baghdad, Baghdad, Iraq

many researchers such as [3–8]. Meyersohn [9] classifies pile failure scheme subjected to the lateral extent of liquefied soil into three categories: (1) deflection as a consequence of soil horizontal displacement causing the pile to reach its bending capacity as shown in Fig. 1a. (2) Buckling due to the absence of lateral support, leading to reduced stiffness of liquefiable soil and imposing lateral deflection which is clearly shown in Fig. 1b. (3) Excessive rigid body rotation, related to large pile diameter and piers as shown in Fig. 1c.

Finally, the pile foundations can buckle under axial loading alone and ignore the influence of lateral loadings during earthquake motions, [10, 11] as shown in Fig. 2. So, many authors such as [12–14] showed that lateral loading has a significant influence on reducing the bucking failure of pile foundations in liquefiable soil.

According to seismic observations, Iraq appears to be vulnerable to seismic risks, [15, 16]. Earthquakes are likely to occur and can inflict significant damage. In fact, similar hazards occurred and were recorded during the November 2017 earthquake [17].

Because of the impact of ships and wind waves, piles in offshore and coastal constructions are not only designed for

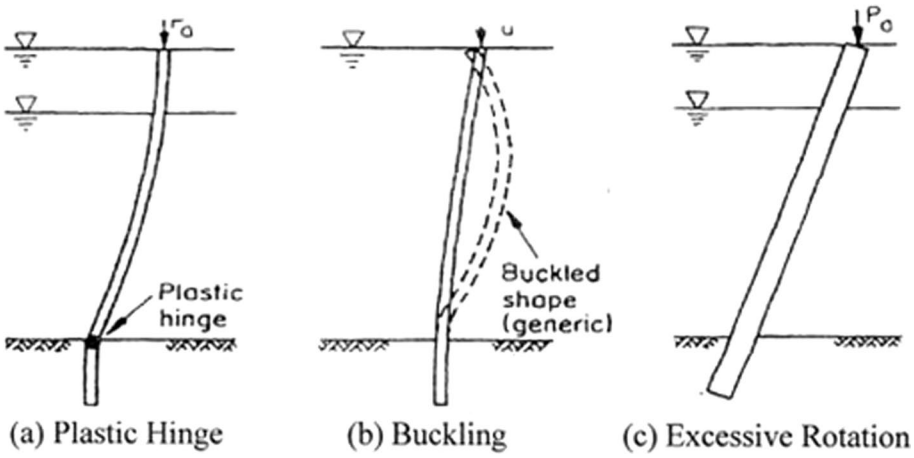

Fig. 1 Pile failure Mechanisms [9]

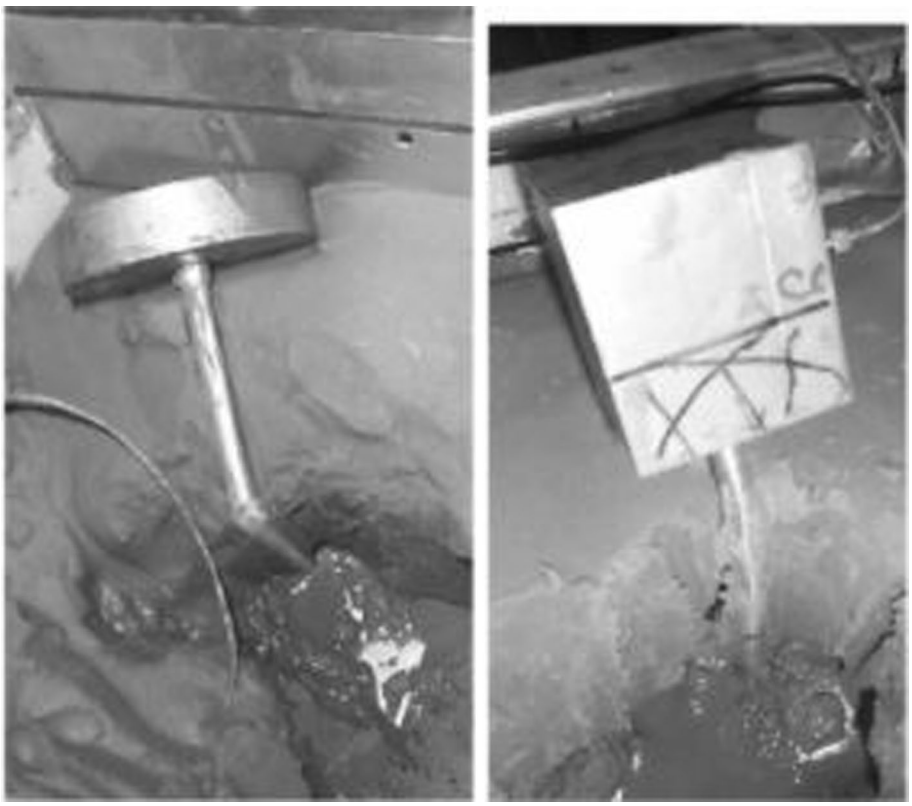

Fig. 2 Buckling of the pile in liquefiable soil, from [12]

axial loading but also for progressive lateral loading [18, 19]. Many researchers studied the mechanism of combined (axial and lateral) loadings on the response of piles in sandy soil by using centrifuge model tests [20] and 1 g model tests [21, 22]. These results show the pile capacity and settlement of the pile foundations are remarkably influenced by lateral loading, while the lateral behavior of the soil is affected by axial loading.

Shaking tables are an essential instrument in earthquake engineering research for examining the behavior of structural components or substructures under dynamic excitations similar to those caused by actual earthquakes. Shaking table tests are used to evaluate theories and predictions, learn about previously undiscovered mechanisms, and investigate the dynamic consequences of specimen performance. As a result, the purpose of this study is to explore the pile response to mixed (axial and lateral) loading conditions in saturated sandy soil when subjecting it to real seismic motions by means of the shaking table device.

Experimental work

Shaking table design and apparatus

Pile response under different conditions of combined (axial and lateral) loading was studied with the aid of the shaking table manufactured by [23]. The shaking table consists a of chassis, two linear guide rails, a Ball screw, Brackets, a Table, Servo Motor, and drive. The shaking table dimension was (800) mm in length and (800) mm in width, which has the ability to produce 1-D horizontal movement along the length direction with the max acceleration of (± 3 g) and mass of (1000) kg, where g is the gravity acceleration in m/s^2. The frequencies of the input motions vary between (0–100) Hz, and the maximum table displacement was (200) mm. The shaking table system is illustrated in Fig. 3. Geometry scaling of the model ratio to the prototype was [1:35] according to [24] illustrated scale factors for different simulated parameters for shaking table studies.

Model box design

The Al-Temeemi [23] laminar shear box has twelve steel square laminae that are layered one on top of the other, and it has rails that allow it to freely glide in one horizontal direction. Figure 4 shows the dimensions of the steel tube used to make the laminae. The laminar shear box had a total height of (838) mm and was constructed as a square frame with outer dimensions of (700*650) mm, inner dimensions of (600*600) mm, and a height of (50) mm for single laminae. Thus, the tested soil model's dimensions were (600*600*600) mm. This eliminates the side friction of the box wall as described in [25, 26] by setting the relevant soil model height-to-width to unity. The coefficient of sliding friction of the laminae was (0.031). Thin linear ball-bearing rail strips with dimensions of (500) mm, (43) mm, and (12.5) mm in height were welded between each lamination [23].

Model soil and pile

The sandy soil was from Karbala city, Iraq, which should be dried and then screened on sieve No. 10 before testing. The soil was placed into the laminar shear box in orders

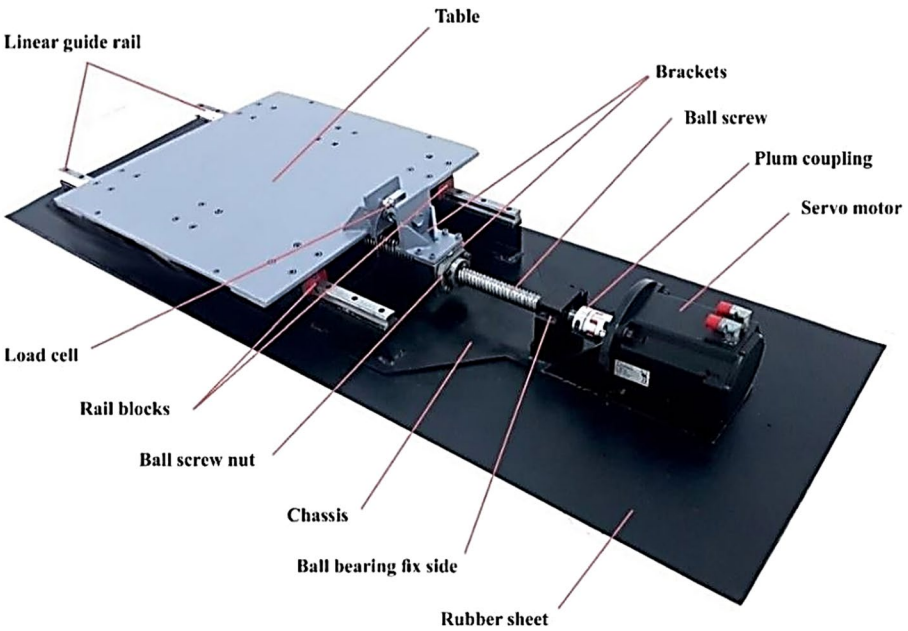

Fig. 3 Shaking table system, from [23]

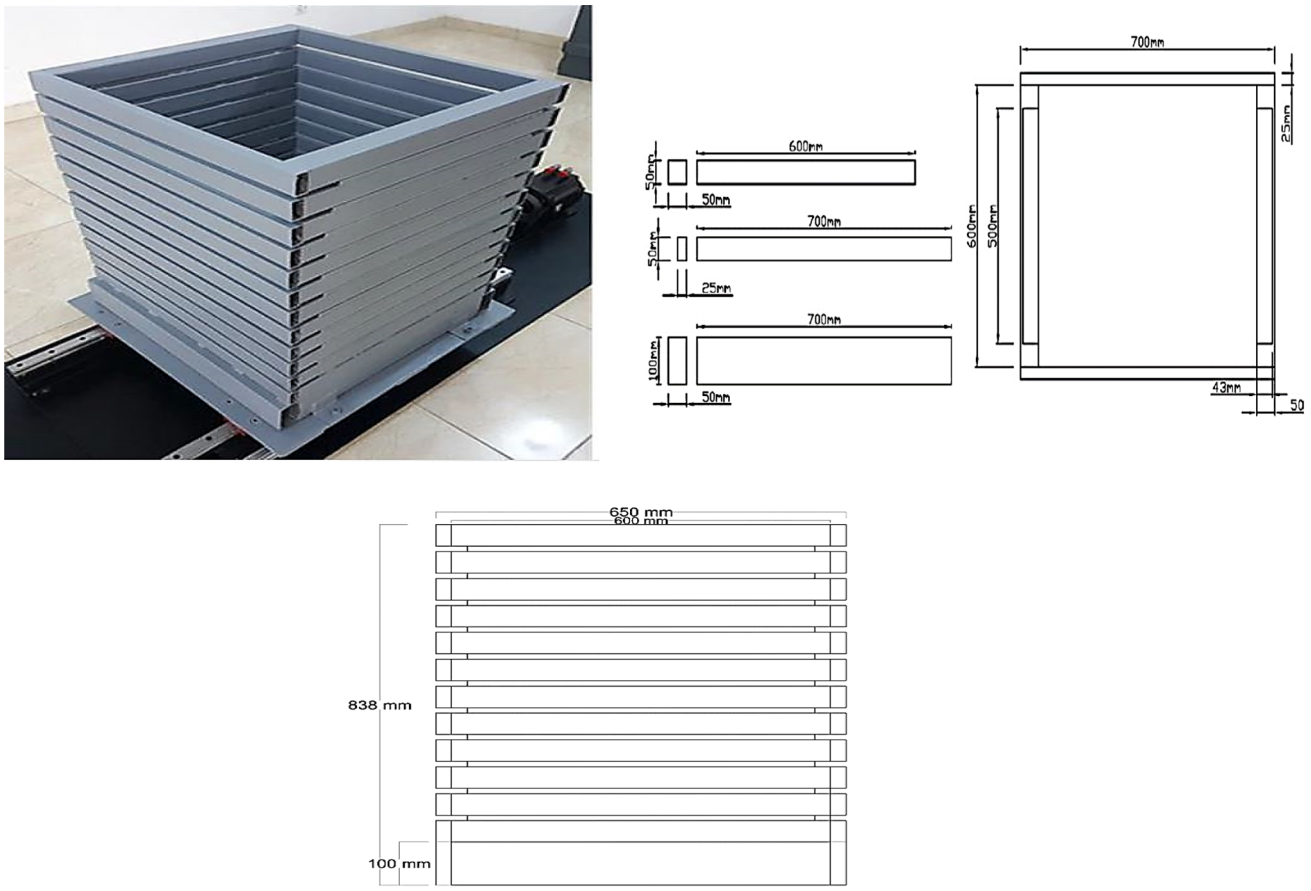

Fig. 4 Laminar shear box [23]

of layers at relative densities (70 and 30) %, respectively, based on tamping and raining technique methods. Table 1 lists the results of soil properties. The model soil consisted of three layers: The first one, made of (320) mm thick loose sandy soil, the middle layer made of (280) mm thick, dense sandy soil, and finally, the filter layer of (150) mm thick was placed at the bottom of laminar shear box system to prevent the soil sample exit during discharge of water. The soil was furnished by an aluminum rod until it becomes homogenous and then lightly compressed by a wooden plater to obtain a flat surface. During the preparation of sand soil, the sensors (accelerometers and pore pressure) are installed in the soil sample with different levels. During the preparation of the soil sample, the single pile is fixed at the center of a laminar shear box. For saturation, the water distribution system is placed at the end of the laminar shear box after connecting

Table 1 Soil physical and mechanical parameters

Index Properties	Values	Index Properties	Values
Initial Relative Densities, (R.D,%)	30–70%	Max. dry unit weight, (kN/m^3)	15.56
Max. dry unit weight, kN/m^3	15.56	Min. dry unit weight (kN/m^3)	13.95
Min. dry unit weight, kN/m^3	13.95	Cohesive coefficient, c	0
Specific gravity, Gs	2.64	The angle of internal fraction, (φ) loose	33°
Maximum void ratio, (e_{max})	0.86	Angle of internal fraction, (φ) dense	36°
Minimum void ratio, (e_{min})	0.66	D_{10}, (mm)	0.14
Coefficient of uniformity, (Cu)	2.92	D_{30}, (mm)	0.35
Coefficient of curvature, (Cc)	2.13	D_{60}, (mm)	0.41
Soil Classification, (USCS)*	SP	Permeability, k (cm/s)	$5.6*10^{-3}$

*USCS: Unified soil classification system

with a tube to supply water from a constant head water tank. After the saturation process, earthquake eve simulator software was executed, earthquake acceleration was selected, and test information was entered. Axial and lateral loading was applied on the pile head. Then, the last accelerometer was fixed on the pile, however, the displacement transducers were linked to the center of the pile head across the screw nut. All sensor's initial readings are subtracted, then the test was started, and the shake was triggered while data from sensors streamed to the DAQ until the shake ended. The pile model used in the research was made from an aluminum alloy pipe, (500) mm in length, with an outer diameter of (16) mm with (L/D) equals to 25 (rigid pile), density (2700) kg/m^3, and young's modulus of (65) GPa.

Instruments

Sensors (e.g., accelerometer, pore water pressure, and lateral and vertical displacement transducers) were used in this research to record various parameters during shaking table tests. Figure 5 illustrates the arrangement of the sensors in the shaking table system. The sensors consisted of (3) accelerometers, one on the pile head and two in the soil strata, (2) pore pressure transducers located in the soil strata, (4) strain gauges along the pile, and (2) lateral and vertical displacement transducers on the pile head model, which were denoted as [Acc, PP, ST, DT2, and DT1], respectively. All sensors were calibrated before the test.

Characteristics of input motions and test cases

A number of shaking table models were efficient in simulating the behavior of a single pile during an earthquake event under various conditions of combined loading on saturated sandy soil. As a result, the Kobe, El-Centro, Halabjah, and Ali Algharbi earthquakes were used. Figure 6 displays the acceleration time histories for four earthquake motions. The information regarding the earthquake motions employed is displayed in Table 2.

The pile head was located (100) mm above the sandy soil surface. Hence, the total pile length of (500) mm. The total allowable axial load capacity was applied by placing a weight block of 2 kg (19.6 N) directly on the pile head. In order to simulate the lateral loading system on the pile head, an automated pneumatic-vacuum loading system was locally manufactured. The lateral loading system encompasses tension loading that is placed on the upper movable laminar shear box, as shown in Fig. 7. The total allowable lateral load capacity equals (20%) of the total allowable axial loading. In this study, six test cases were considered in the shaking table model, as shown in Table 3. In (A6, H6. E6, K6, A5, H5, E5, and K5) case tests, the only axial load was applied on the pile, while the other test cases were represented combined (axial and lateral) loading through different earthquake motions.

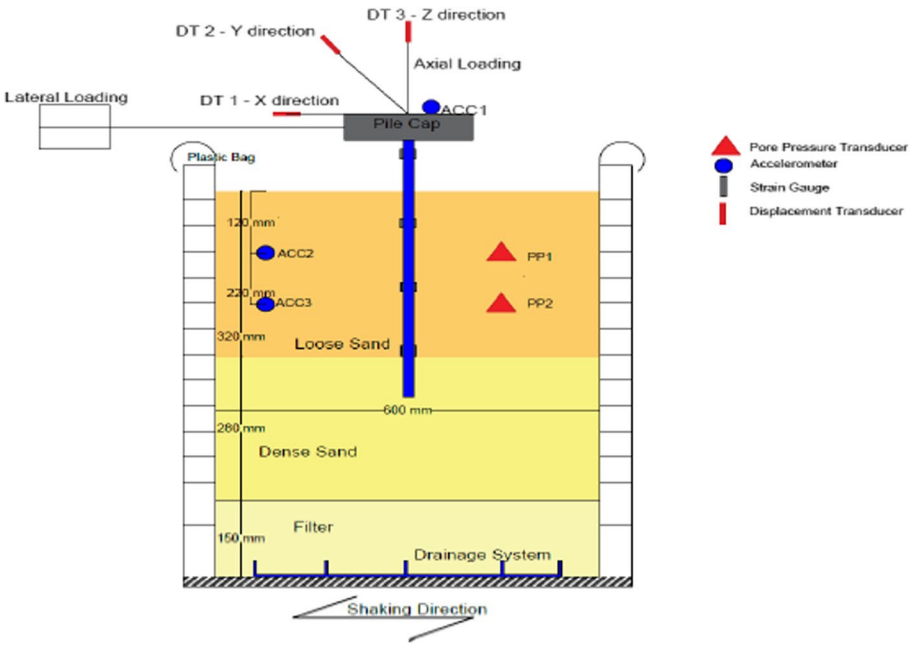

Fig. 5 Testing model layout

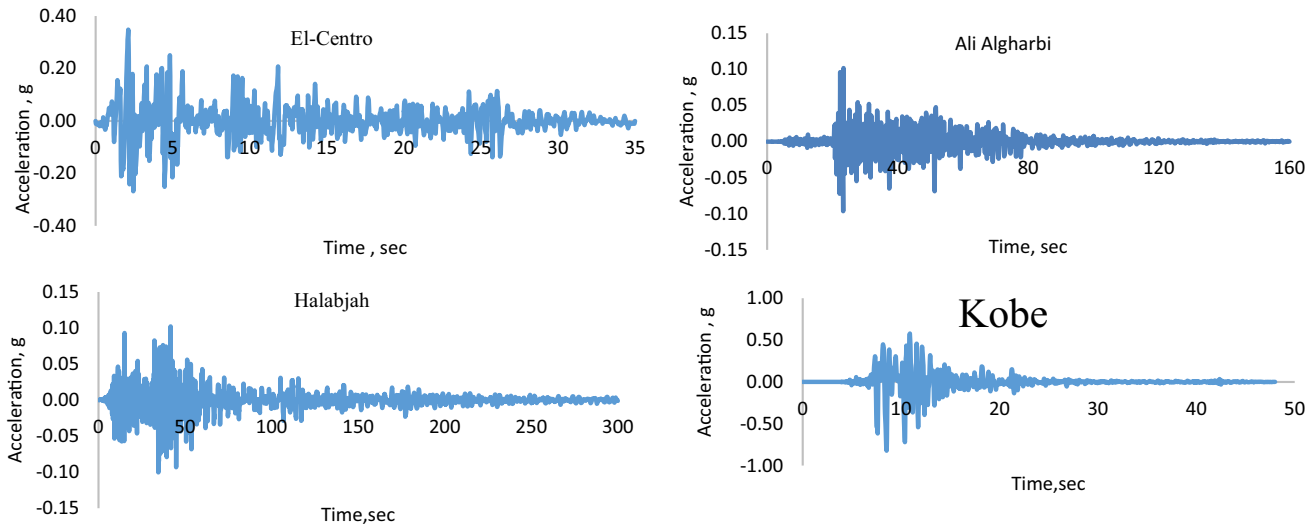

Fig. 6 Acceleration history with time for earthquake motions

Table 2 Information for the earthquake data

Earthquake	Ali Algharbi	Halabjah	El-Centro	Kobe
Region	Iraq	Iraq-Iran border	California-USA	Japan
Magnitude, (Mw)	4.9	7.3	6.9	6.9
Modified Mercalli intensity	Weak	Moderate to heavy	Extreme	Very strong
Shake duration, (sec)	160	300	35	48
Frequency,(Hz)	10	10	50	50
Acceleration, (g)	0.1	0.1	0.35	0.82
Acceleration direction	N-S	E-W	N-S	N-S
Data	25-9-2015	12-11-2017	19-5-1940	16-1-1995
Epicenter depth, (km)	10.0	19.0	8.8	17.9
References	Iraqi Meteorological Organization and Seismology	Iraqi Meteorological Organization and Seismology	www. Strong motion cemter.org	www. Strong motion cemter.org

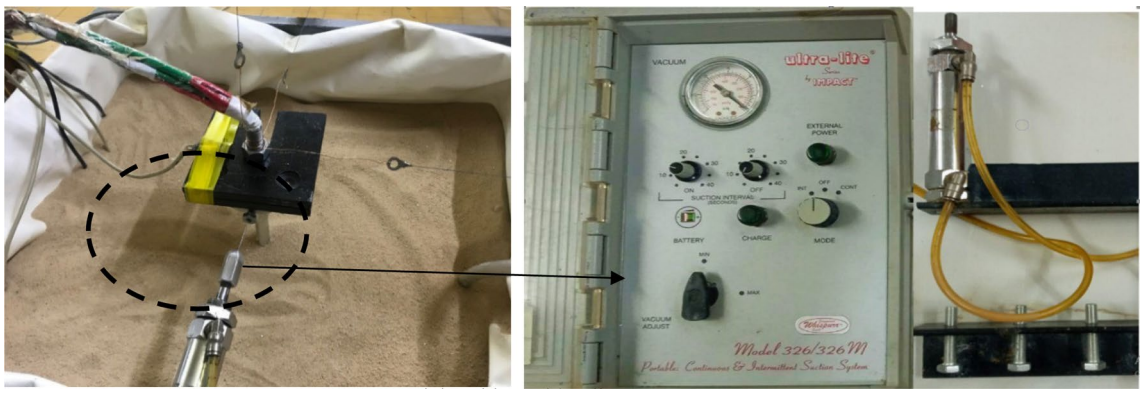

Fig. 7 Setup model and lateral loading system

Table 3 Tests cases for the shaking table tests

Code	Description	Code	Description	Code	Description	Code	Description	Code	Description
A1	Ali-Algharbi 50 axial, 50% lateral	A2	Ali-Algharbi 50% axial, 100% lateral	A3	Ali-Algharbi 100% axial, 50% lateral	A4	Ali-Algharbi 100%axial, 100%lateral	A5	Ali-Algharbi 100% axial, 0 lateral	A6	Ali-Algharbi 50% axial, 0 lateral
H1	Halabjah 50 axial, 50% lateral	H2	Halabjah 50% axial, 100% lateral	H3	Halabjah 100% axial, 50% lateral	H4	Halabjah 100%axial, 100%lateral	H5	Halabjah 100% axial, 0 lateral	H6	Halabjah 50%, axial, 0 lateral
E1	El-Centro 50 axial, 50% lateral	E2	El-Centro 50% axial, 100% lateral	E3	El-Centro100% axial, 50% lateral	E4	El-Centro100%axial, 100%lateral	E5	El-Centro 100% axial, 0 lateral	E6	El-Centro 50% axial, 0 lateral
K1	Kobe 50% axial, 50% lateral	K2	Kobe 50% axial, 100% lateral	K3	Kobe 100% axial, 50% lateral	K4	Kobe 100% axial, 100% lateral	K5	Kobe 100% axial, 0 lateral	K6	Kobe 50% axial, 0 lateral

Interpretation of test results

Acceleration response of pile head and soil

Figures 8, 9, 10 and 11 show the acceleration time histories measured at the pile head with different earthquake motions under combined loadings. It can be noted for a low earthquake motion of Ali Algharbi and Halabjah, an increase in axial loading, the measured peak acceleration was increased from 0.187 and 0.185 g for cases A6 and H6, respectively, to 0.219 and 0.199 g, irrespective of A5 and H5, in contrast, this behavior, with combined loading and inclusion of lateral load, the recorded acceleration at peak time will generally be reduced to 0.136 and 0.179 g when 50% of lateral load is included for Ali Algharbi with A1 and A3 as well as 0.145 and 0.152 g for Halabjah at H1 and H3, respectively. Hence, a further increase to 100% additionally reduces measured acceleration for both motions to peak values of 0.118, 0.145, 0.15, and 0.13 g for A2, A4, H2, and H4. Near the beginning of the El-Centro earthquake, it is found that the peak acceleration of the pile was mainly controlled by the input acceleration possessing larger head masses, the acceleration values ranged between 0.364 and 0.449 g at E6 and E5, while limited reduction values ranged between 10% when combined loading reached 50% and 14% at 100% for both cases E2 and E4. When the soil liquefies occur, the liquefaction works to dampen the earthquake power and de-amplification the earthquake acceleration. From the results, it can be shown the increase of combined loadings reaching 50% for cases K1 and K3 will reduce the peak acceleration by the average value of 6% than at 100%, the same trend was noticed. This peak gradually reduced to 9% of the peak when dealing with K2 and K4, this scenario could be attributed to the fact, that the soil layer is liquefied, losing lateral soil support, and the energy of the vertically propagating shear waves will, to a certain degree, be absorbed by the liquefied soil.

In general, the peak acceleration on the pile head gradually increases through different four earthquake motions and the time to reach peak acceleration is consistent with the time when the input earthquake motion reaches the peak. The results indicated that as the axial load increase, the peak acceleration decrease at the pile head. Hence, these results are well associated with the finding of [22]. Under combined loading, it is worth noting that there is a significant decrease in peak acceleration values as lateral loading increases.

Hence, this effect was apparent for A4, H4, and E4 by reducing the values by 22%, 23%, and 18%, respectively. While in the Kobe earthquake, the common behavior shows a slight reduction in the peak acceleration at pile head load. This behavior could be attributed to the minor effect of lateral loading resistance during the excitation of strong motion.

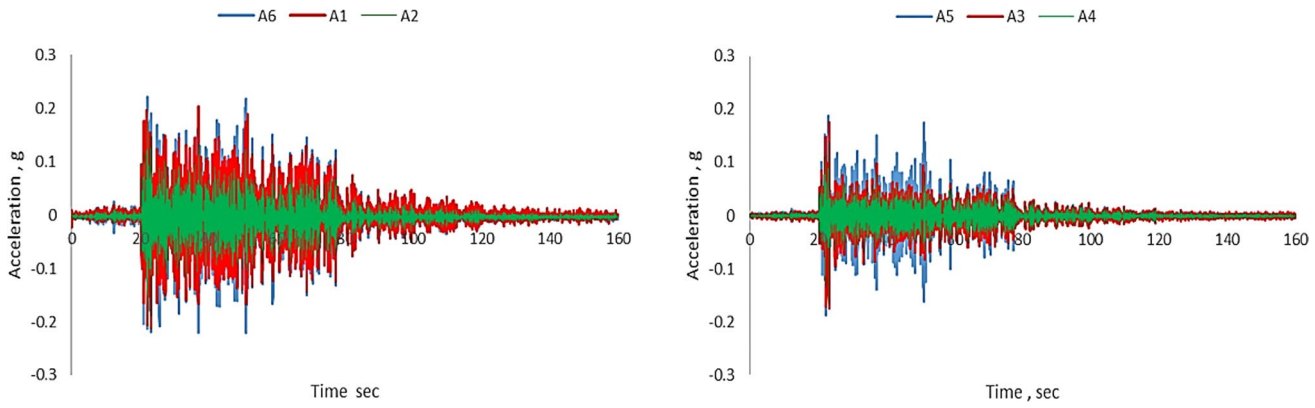

Fig. 8 Acceleration time history of the pile head during Ali Algharbi earthquake

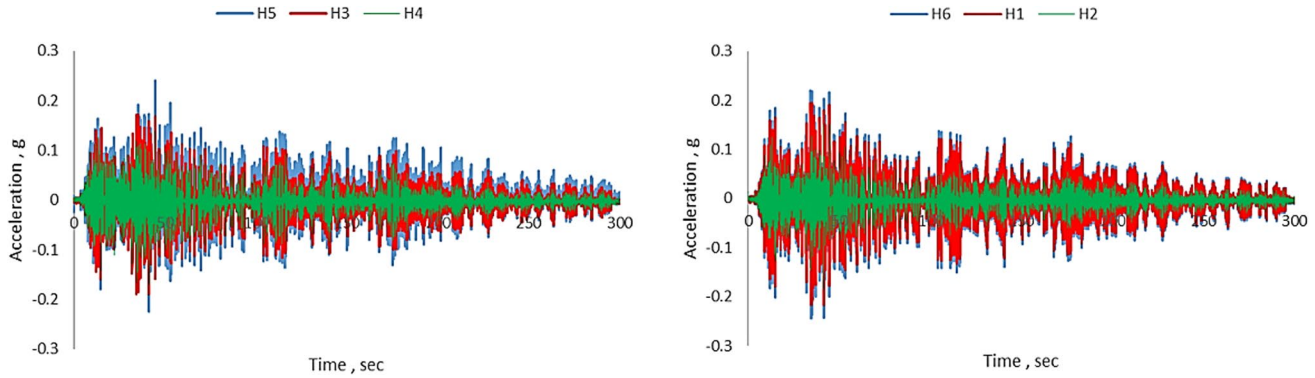

Fig. 9 Acceleration time history of the pile head during Halabjah earthquake

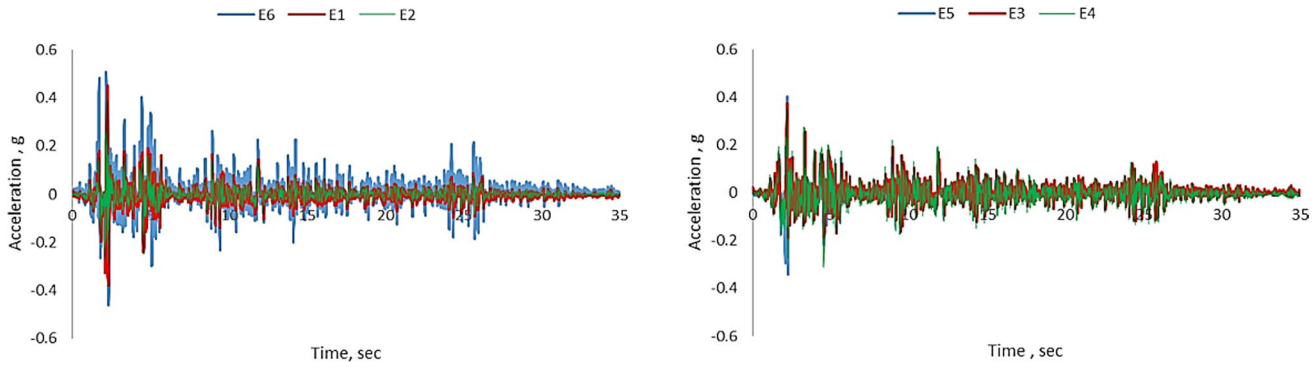

Fig. 10 Acceleration time history of the pile head during El-Centro earthquake

Figures 12 and 13 present the variation of peak acceleration at the pile head and soil strata for all earthquake motions. It can be inferred that, in weak to extreme earthquake motions, the peak acceleration slightly decreases within soil strata. However, the acceleration history exhibited a gradual increase in an upward direction in a loosely liquefied layer depth.

It should be noted, for strong motion, the peak acceleration at the pile head appears highly concerning soil strata this lies behind the fact of filtration and rapid generation of pore water pressure that destroyed the soil skeleton, [14, 17]. From the results mentioned above, the combined loading has a major effect on the reduction of peak acceleration at the pile head in weak to extreme earthquake motion and

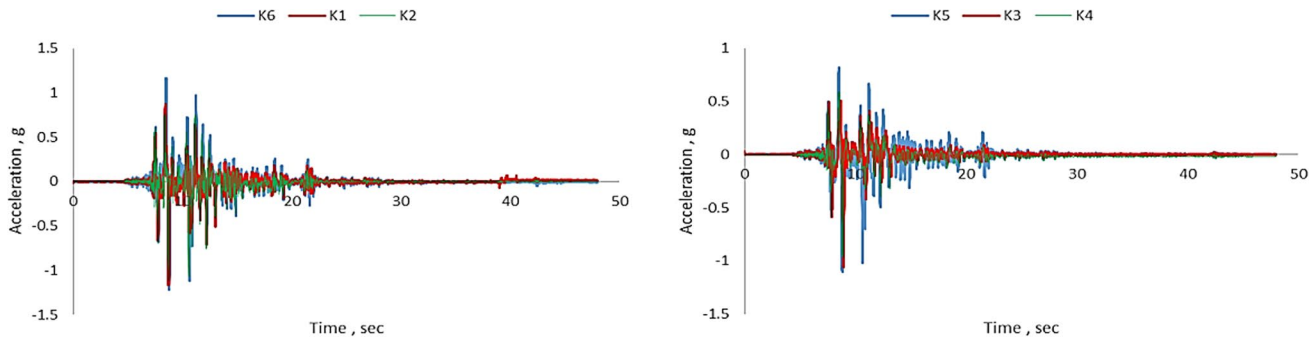

Fig. 11 Acceleration time history of the pile head during the Kobe earthquake

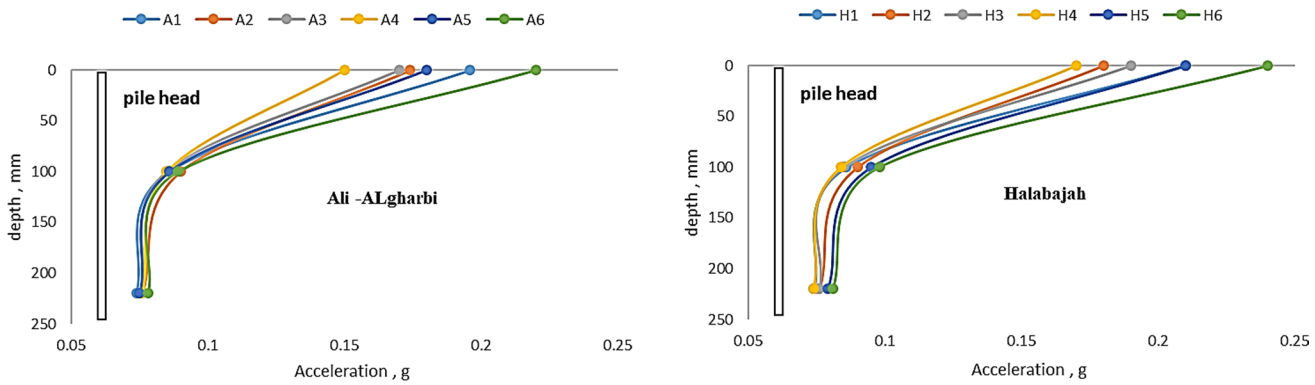

Fig. 12 Variation of peak acceleration at pile head and soil strata for Ali Algharbi and Halabjah earthquakes

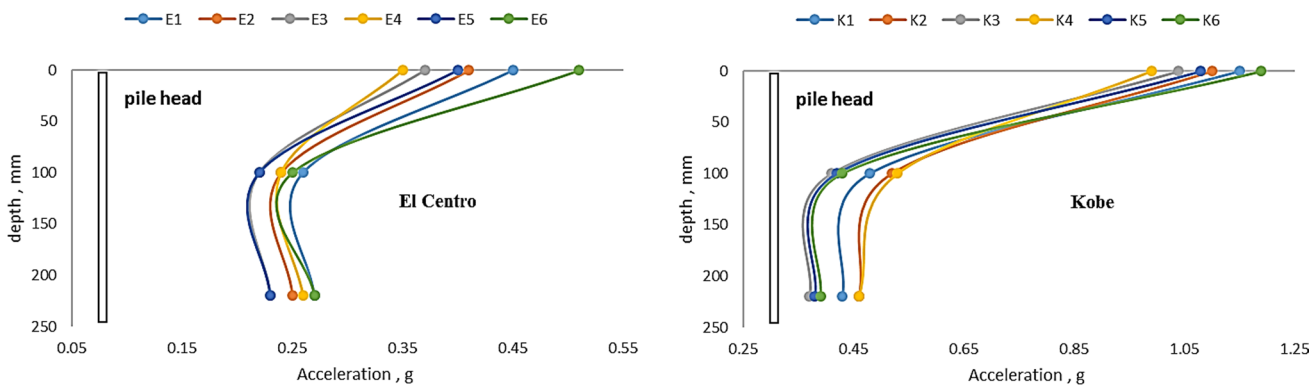

Fig. 13 Variation of peak acceleration at pile head and soil strata for El-Centro and Kobe earthquakes

a minor effect in strong motion; on the other hand, it has a slight effect on the peak acceleration in soil strata.

Lateral displacement at the pile head

Figures 14, 15, 16 and 17 illustrate the variation of lateral displacement on the pile head with time. It is observed that the lateral displacement increases as peak acceleration increases. The maximum lateral displacement of the pile head rounded about (4.68, 18.95, 23.59, and 68.30) mm for A5, H5, E5, and K5, respectively, while (3.67, 7.65, 10.43, and 67.18) mm for A6, H6, E6, and K6. From the results, it can be concluded the lateral displacement on the pile head increases along with the increasing axial loading. The relationship between the lateral load and lateral displacement of the pile head for all test cases under constant static axial loadings is shown in Fig. 18. It can be observed that for the constant static axial loading, the lateral displacement

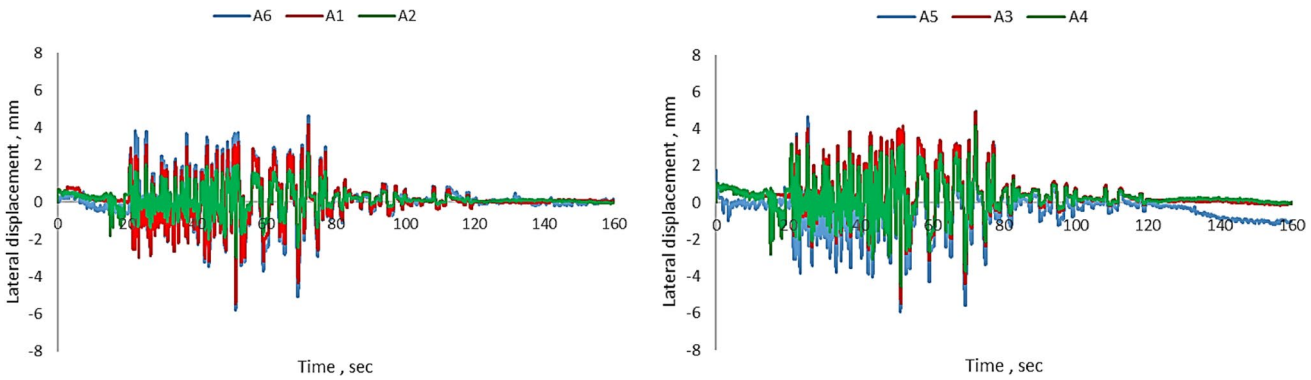

Fig. 14 Lateral displacement time history of the pile head during the Ali Algharbi earthquake

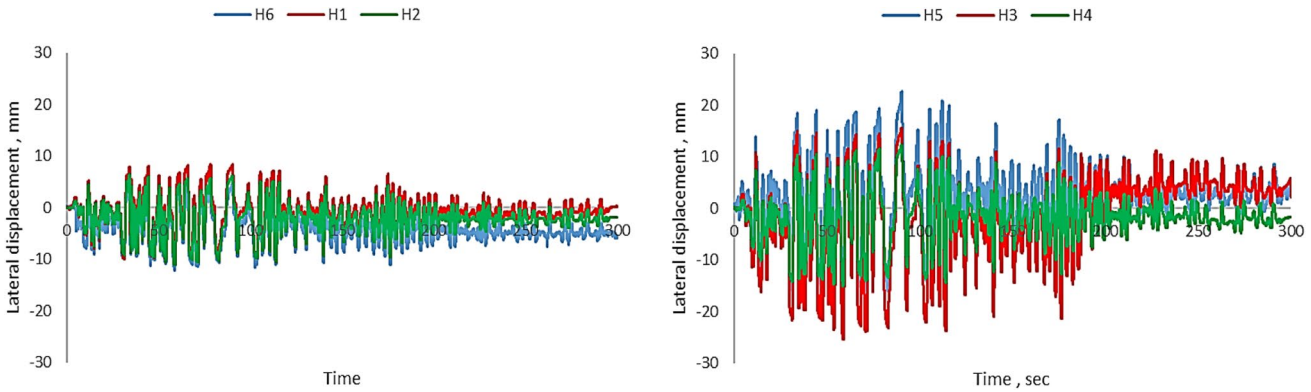

Fig. 15 Lateral displacement time history of the pile head during the Halabjah earthquake

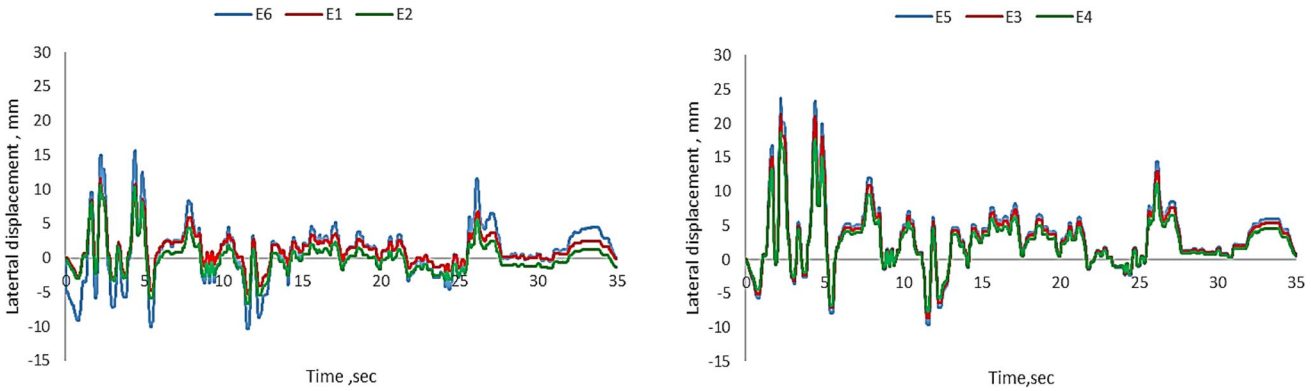

Fig. 16 Lateral displacement time history of the pile head during the El-Centro earthquake

decreases with increasing static lateral loading through different earthquake motions. Lateral loading has been a significant effect on lateral displacement by reducing head displacement, for instance (34, 44, 21, and 17) % for A4, H4, E4, and K4 when compared with test cases A5, H5, E5, and K5. These results indicate an inverse relation, as static lateral loading increase the pile head displacement decrease concerning static axial loading for weak to moderate earthquake. In this aspect, the static lateral loading appears to act as a damper on the incidence of lateral motion. However, because of the high acceleration of these motions, they have less of an effect on lateral pile reaction when subjected to extremely powerful earthquake events, i.e., the effect of acceleration is greater than the effect of static lateral load.

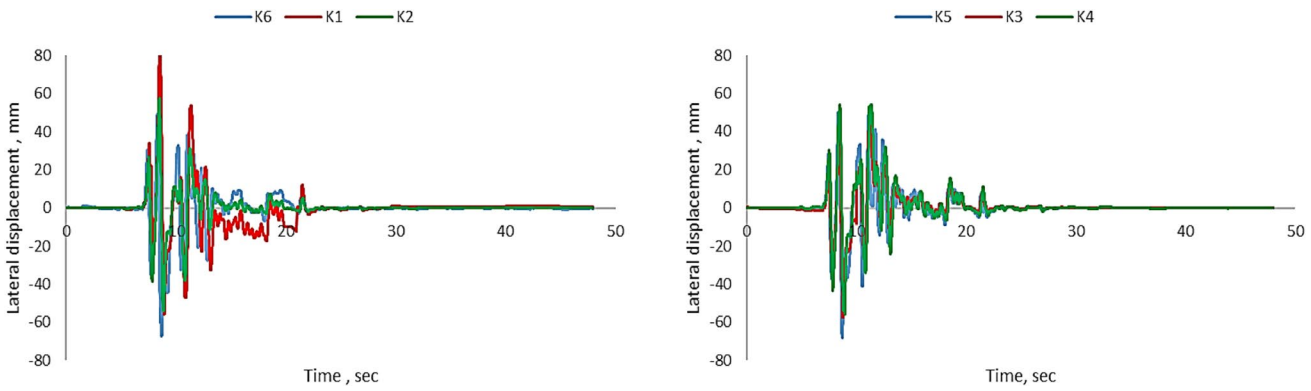

Fig. 17 Lateral displacement time history of the pile head during the Kobe earthquake

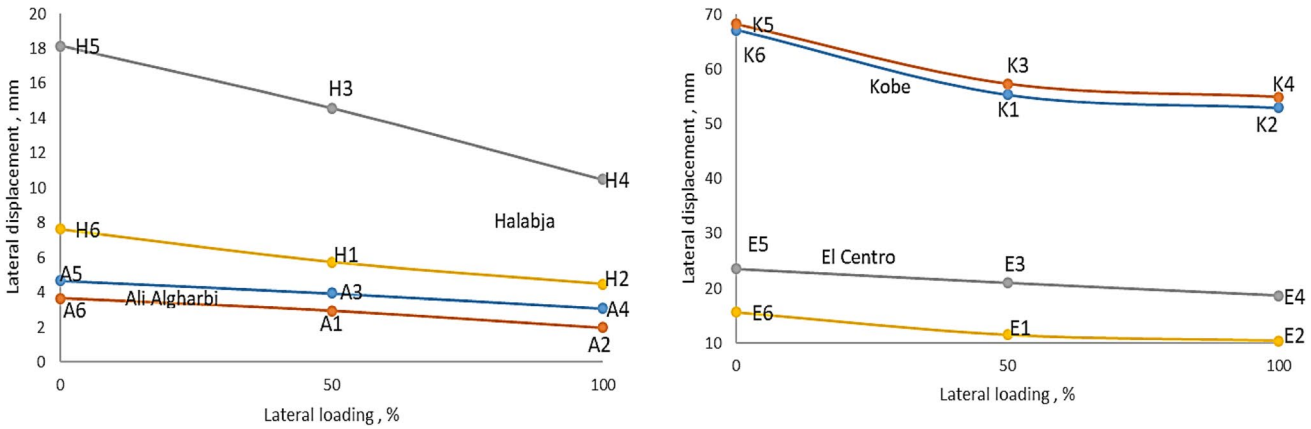

Fig. 18 Relationship between the lateral displacement at pile cap and static lateral loading percent for four earthquake motions

Pile behavior during shaking table testing with and without static lateral loading is briefly described in Fig. 19, considering two cases (H5 and H4). It can be noted that the inclusion of lateral loading may interpret the difference in pile behavior in both cases H4 and H5. It is observed that noticeable rotation occurred in the pile after shaking. This type of pile failure may be due to pile rigidity, similar to behavior found by [9].

Distribution of Rotation along with the pile depth

The relationship between the lateral load and rotation along the pile for all test cases under constant static axial loadings is shown in Fig. 20. It can be observed that for the constant static axial loading, the rotation of the pile decreases with increasing static lateral loading through different earthquake motions. In general, it can be shown that input motion intensity increases, and the peak rotation increases. From the results, it has appeared that with the increasing combined loading, the pile likely showed low rotation value due to the lateral restraint effect and reduction in axial load as a result of the inertial force generated at the pile head.

Vertical displacement at the pile head

The time histories of vertical displacement on the pile head are shown in Figs. 21 and 22 and all test cases value is listed in Table 4. The maximum values of the vertical displacement were equaled (1.40, 9.90, 10.98, and 24.20) mm for A4, H4, E4, and K4, respectively. The test case results indicated that the little increase in vertical displacement values due to the lateral loading suddenly increased during the initial lateral loading stage and tended to be stable in all tests. Hence, it can be concluded the vertical displacement of the pile head due to lateral loading that is clearly associated with pure axial loading for all test cases. However, in shaking table tests, the settlement may require more time since it is related to inducing pore water dissipation, besides it may be tolerated error value for seismic loading, [27].

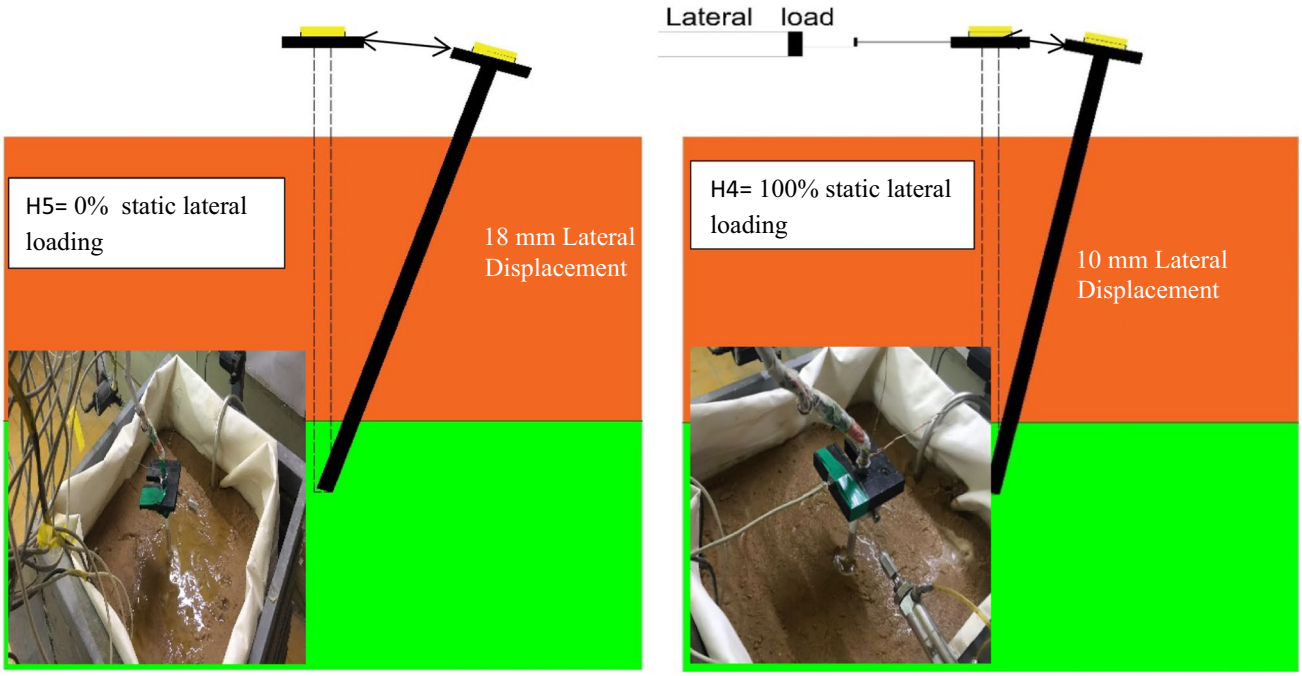

Fig. 19 Pile behavior after shaking test H5 and H4 with and without lateral loading

Soil liquefaction characteristics

The liquefaction phenomenon is defined in terms of a generation of excess pore water pressure and reduced soil initial vertical stress. First, in order to investigate the possibility of liquefaction occurrence during earthquakes, a magnitude of (ru) is calculated. The (ru) is defined as the soil in the liquefaction state, where is the difference between the current and hydrostatic pore pressure, and (σv_o) is the initial effective vertical stress as stated in Eq. 1.

$$\mathrm{ru} = \frac{\Delta u}{\sigma v_o} \tag{1}$$

History of pore water pressure ratio with time presented in Figs. 23, 24, 25 and 26 in loosely sandy soil strata. It has appeared that the excess pore water pressure gradually increases within soil depth among all earthquake motions. In the Ali Algharbi earthquake, the occurrence of initial liquefaction seems unclear since the average maximum pore pressure ratio, ru reaches 0.91 and 0.85, respectively, at (100) mm and (220) mm of soil depth at the time of 20 secs, these findings coincide with [23, 28, 29]. On the other hand, the soil exhibited initial liquefaction after 37 s of shaking. Furthermore, no liquefaction potential could experience during El-Centro earthquake, since the ru values reach 0.84, and 0.88, respectively, at the time of 3 secs, during the Kobe earthquake, the pore pressure ratio will generate and build up rapidly exceeding the value of 1. The excess pore pressure may experience a large increase and slower dissipation in a strong earthquake could be attributed to the effect of earthquake acceleration. These findings coincide with those [19]. Finally, axial loading has a noticeable influence in the reduction of pore water pressure and densification of soil liquefaction in medium sandy soil, but, in loose sandy soil, this influence is insignificant except for extensive large loading, [8]. Besides, it can be concluded that the lateral loading on the pile head does not have a noticeable effect on excess pore water pressure and pore pressure ratio under different all of the four earthquake motions.

Conclusions

1. It should be noticed from the shaking table experiments that for significant motion, the peak acceleration at the pile head appears to be very problematic soil strata. This is what caused the filtration and quick buildup of pore water pressure, which damaged the soil skeleton. According to the results, combined (axial and lateral) loading results in a significant reduction of peak acceleration at the pile head for light earthquake motion and a minor reduction for strong earthquake motion. However, it has a minor effect on the peak acceleration of the soil strata.
2. As static lateral loading increase the pile head displacement decrease concerning static axial loading for weak to moderate earthquake. In this aspect, the static lateral

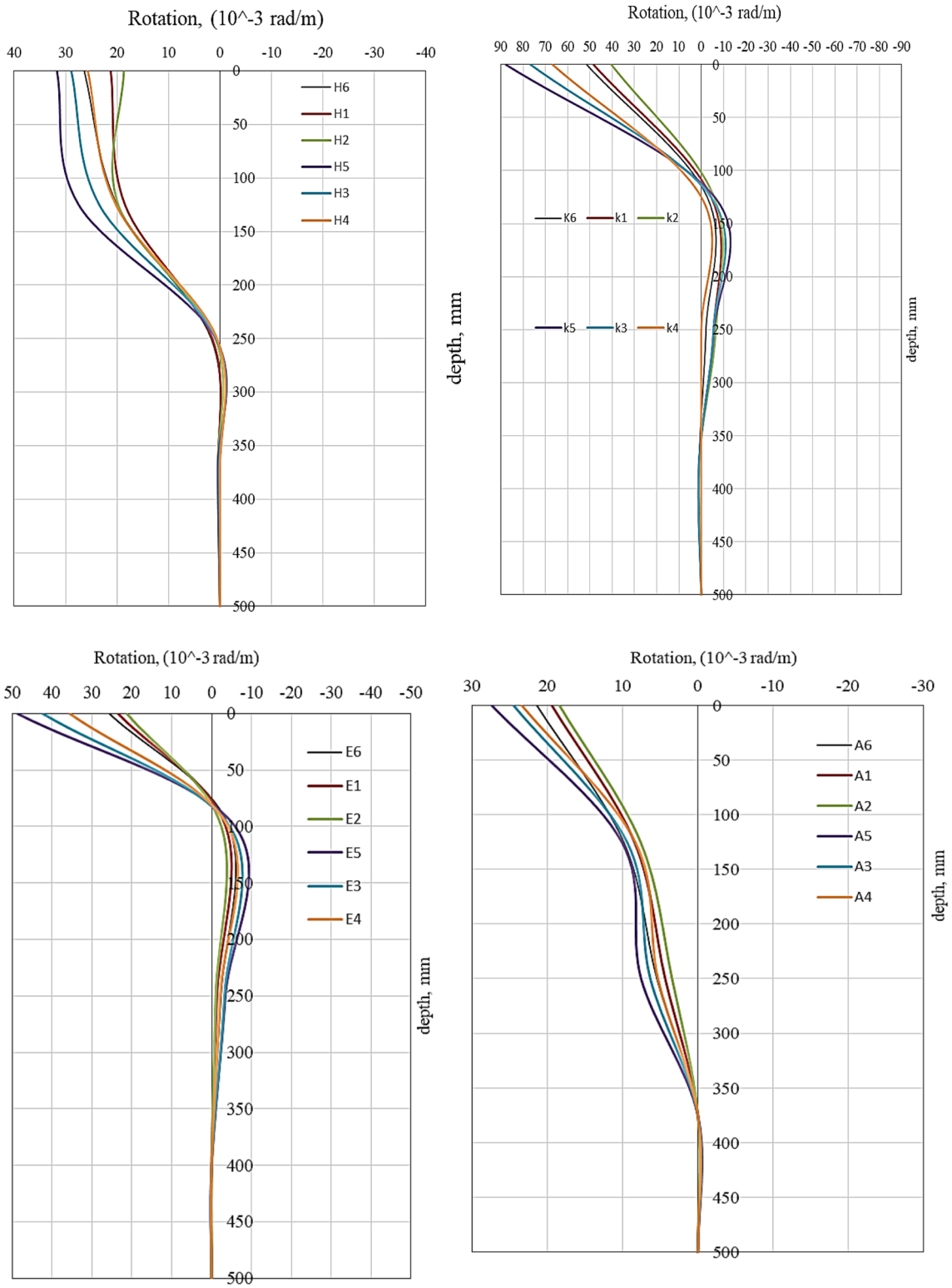

Fig. 20 Rotation along the pile for all earthquakes

loading appears to act as a damper on the incidence of lateral motion. However, because of the high acceleration of these motions, they have less of an effect on lateral pile reaction when subjected to extremely powerful earthquake events, i.e., the effect of acceleration is greater than the effect of static lateral load.

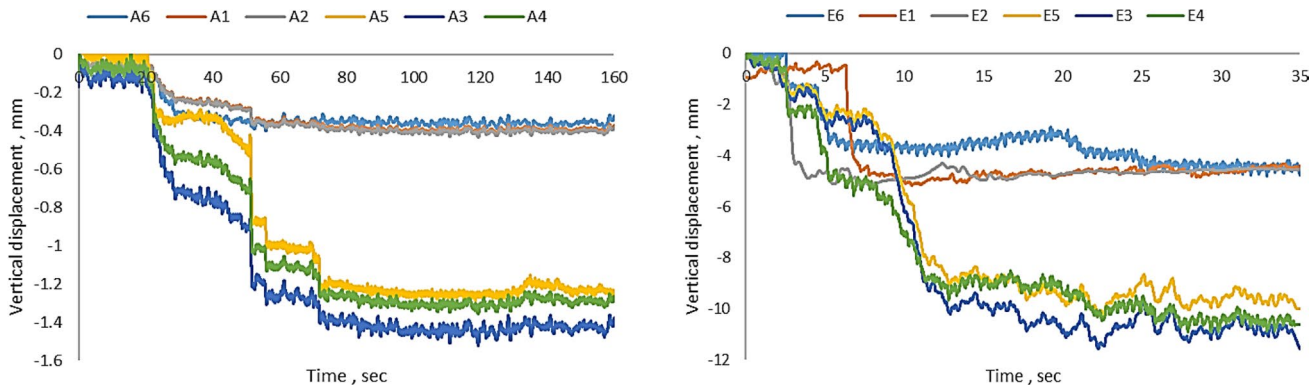

Fig. 21 Vertical displacement on the pile head for Ali Algharbi and El-Centro earthquakes

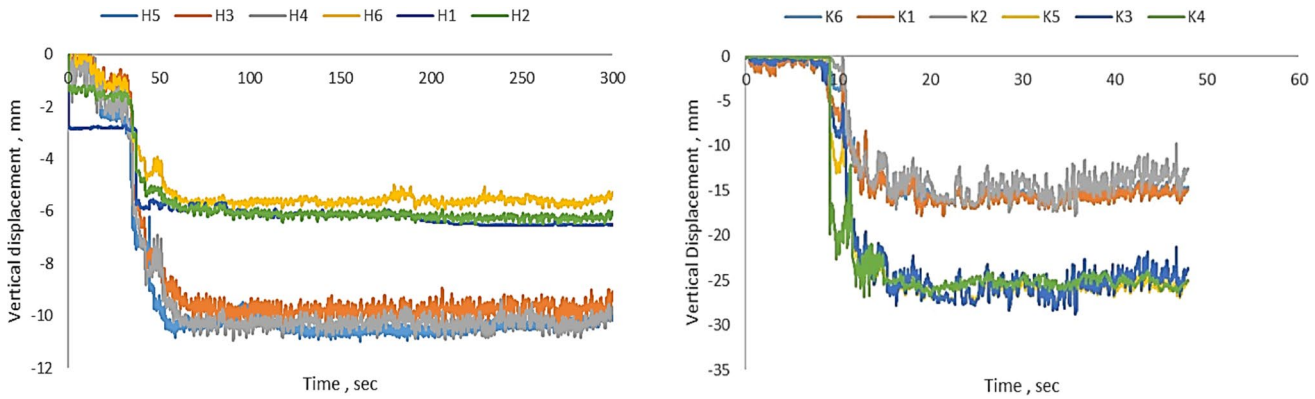

Fig. 22 Vertical displacement on the pile head for Halabjah and Kobe earthquakes

Table 4 Vertical displacements on pile head for test cases, (unit: mm)

Test case type	Vertical displacement	Test case type	Vertical displacement	Test case type	Vertical displacement	Test case type	Vertical displacement
A1	0.38	H1	5.88	E1	4.52	K1	14.40
A2	0.45	H2	5.90	E2	4.62	K2	14.80
A3	1.40	H3	9.85	E3	10.90	K3	24.20
A4	1.38	H4	9.90	E4	10.98	K4	24.70
A5	1.35	H5	9.80	E5	10.80	K5	23.90
A6	0.35	H6	5.82	E6	4.01	K6	13.58

3. The rotation value decrease with increasing the lateral loading on the pile head, especially in low earthquake motions, while in a strong earthquake, the soil around the pile starts to fail quickly, causing a redistribution of the soil lateral pressure along the top of the pile head, consequently the lateral loading will reduce the rotation value.
4. As the combined loading increases, the vertical displacement increases until it reaches a constant value; this increment is related to the axial loading and the intensity of earthquakes from weak to strong input motions [0.1 g Ali Algharbi, 0.102 g Halabjah to 0.34 g El-Centro, and 0.82 g Kobe]
5. In medium sandy soil, axial loading has a noticeable effect on pore water pressure reduction and soil densification; however, in loose sandy soil, this effect is minimal unless for extensive big loading. Furthermore, it is concluded that lateral stress on the pile head has

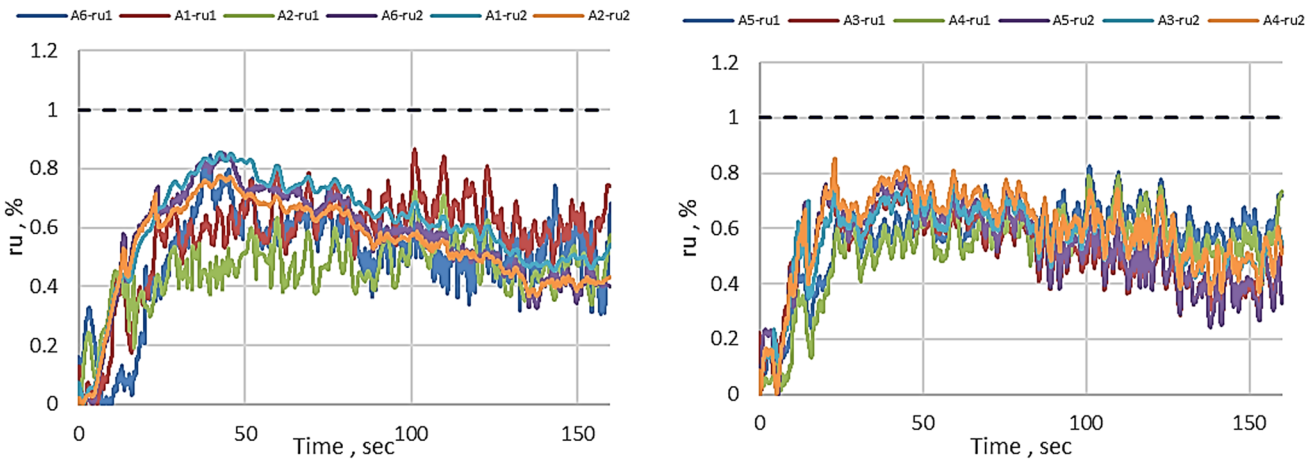

Fig. 23 Variation of pore water pressure ratio with time for Ali Algharbi earthquake

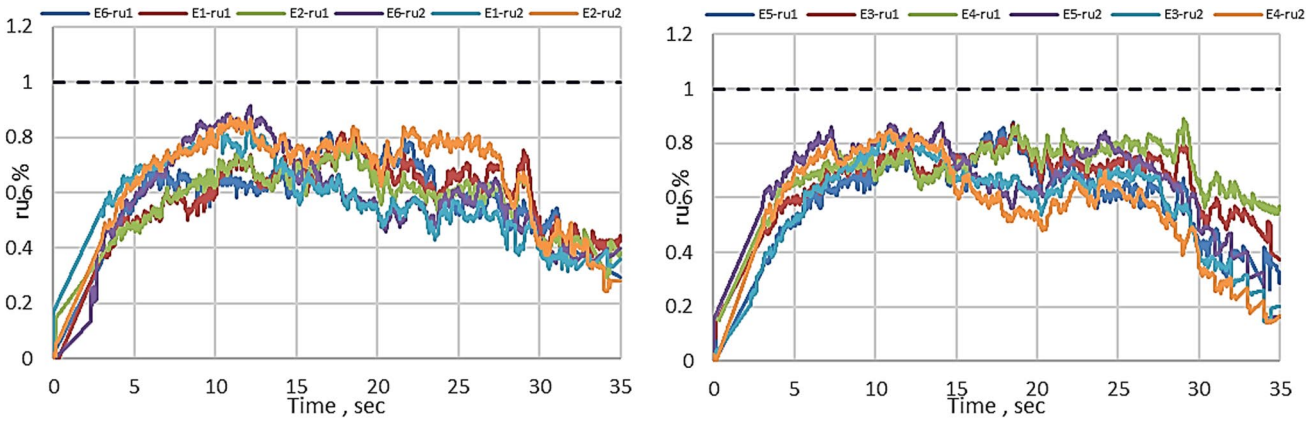

Fig. 24 Variation of pore water pressure ratio with time for El-Centro earthquake

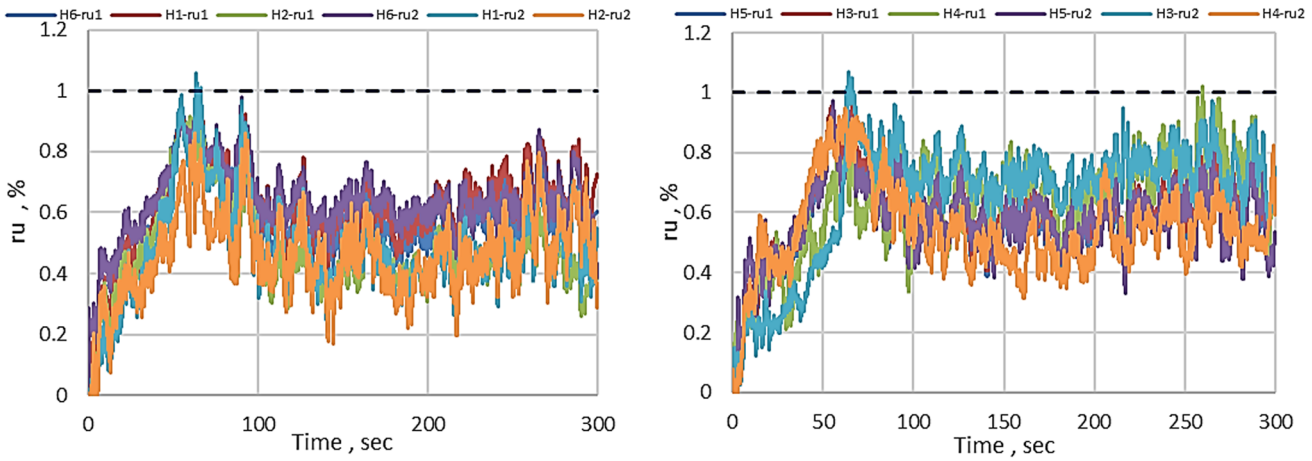

Fig. 25 Variation of pore water pressure ratio with time for Halabjah earthquake

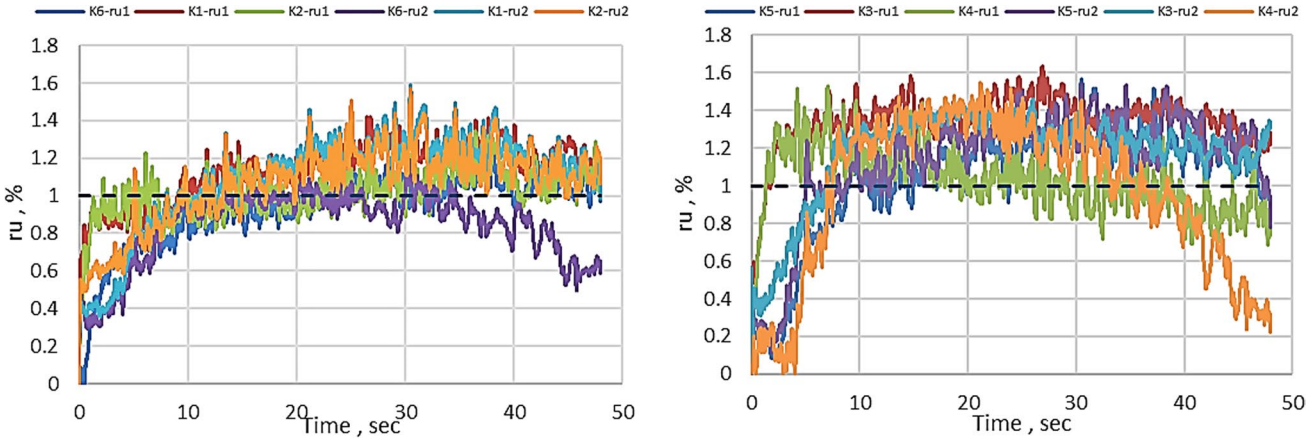

Fig. 26 Variation of pore water pressure ratio with time for Kobe earthquake

no noticeable impact on excess pore water pressure and pore pressure ratio for the four earthquake motions.

6. The results show that the existence of the liquefied soil did not significantly affect the time history of the acceleration of the pile cap and increased the pile cap displacement.

Author contributions All the authors have read and approved the manuscript. The first author, R.S., conduct the experimental testing of the physical model and writing of the manuscript. The second author, B.S., did the analysis, discussion of results, and revised the manuscript.

Availability of data and materials All presented data are available from the corresponding author on reasonable request.

Declarations

Conflict of interest The authors have no conflicts of interest to declare that are relevant to the content of this article.

Ethical approval This article does not contain any studies with human participants or animals performed by any of the authors.

Informed consent For this type of study, formal consent is not required.

References

1. Bao L (2017) Research on lateral dynamic response of pile foundation in liquefiable soil based a on non-linear pseudo-static analysis method. Chem Eng Trans 59:493–498
2. Liyanapathirana D, Poulos H (2005) Pseudo static approach for seismic analysis of piles in liquefying soil. J Geo Geo-env Eng 131(12):1480–1487
3. Bhattacharya S, Madabhushi S, Bolton M (2002) An alternative mechanism of pile failure in liquefiable failure in liquefiable deposits during earthquakes. Tech Rept Univ Camb CUED/D-SOILS/TR324
4. Broms B (1964) Lateral resistance of piles in cohesionless soils. J Soil Mech Found ASCE 90(3):123–156
5. Finn W, Fujita N (2002) Piles in liquefiable soils: seismic analysis and design issues. Soil Dyn Earth Eng 22:731–742
6. Abdoun T, Dorby R (2002) Evaluation of pile foundation response to lateral spreading. Soil Dyn Earth Eng 22:1051–1058
7. Al-Jeznawi D, Ismacahyadi Bagus MJ, Albusoda BS, Norazlan K (2022A) The slenderness ratio effect on the response of closed-end pipe piles in liquefied and non-liquefied soil layers under coupled static-seismic loading. J Mech Behav Mater 31(1):83–89. https://doi.org/10.1515/jmbm-2022-0009
8. Al-Jeznawi D, Ismacahyadi Bagus MJ, Albusoda BS, Norazlan K (2022B) Numerical modeling of single closed and open-ended pipe pile embedded in dry soil layers under coupled static and dynamic loadings. J Mech Behav Mater 31(1):587–594. https://doi.org/10.1515/jmbm-2022-0055
9. Meyersohn W (1994) Pile response to liquefaction-induced lateral spread. Ph.D. Thesis, Civil Engineering Department, Cornel University, and Ithaca
10. Dash S, Bhattacharya S, Blakeborough A (2010) Bending-buckling interaction as a failure mechanism of piles in liquefiable soils. Soil Dyn Earthq Eng 30:32–39
11. Zhang X, Tang L, Li X, Ling X, Chan A (2020) Effect of the combined action of lateral load and axial load on the pile instability in liquefiable soils. Eng Strut 205:110–174
12. Bhattacharya S, Carrington T, Aldridge T (2005) Buckling considerations in pile design. In: Proceedings of international symposium frontiers in Offshore Geots, pp 815–821
13. Almashhadany OY, Albusoda BS (2014) Effect of allowable vertical load and length/ diameter ratio (l/d) on behavior of pile group subjected to torsion. J Eng 20(12):13
14. Chen G, Chen S, Qi C, Du X, Wang Z, Chen W (2015) Shaking table tests on a three-arch type subway station structure in a liquefiable soil. Bult Earthq Eng 13(6):1675–1701
15. Al-Taie A (2015) Profiles and geotechnical properties for some Basra soils. Al-Khwarizmi Eng J 11(2):74–85
16. Albusoda B (2016) Engineering assessment of liquefaction potential Baghdad soil under dynamic loading. J Eng Dev 20(1):59–76
17. Al- Taie A, Albusoda B (2019) Earthquake hazard on Iraqi soil: Halabjah earthquake as a case study. Geodesy Geodyn 10(3):196–204
18. Albusoda B, Alsaddi A (2017) Experimental study on performance of laterally loaded plumb and battered piles in layered sand. J Eng 23(9):23–37
19. Wang X, Ye A, Ji B (2019) Fragility-based sensitivity analysis on the seismic performance of pile-group-supported bridges

in liquefiable ground undergoing scour potentials. Eng Strut 198:109427. https://doi.org/10.1016/j.engstruct
20. Lu W, Zhang G (2018) Influence mechanism of vertical-horizontal combined loads on the response of a single pile in sand. Soils Found 58(5):1228–1239
21. Zhao C, Liu F, Qiu Z, Zhao C, Wang W (2015) Study on bearing behaviour of a single pile under combined vertical and lateral loads in sand. Chin J Geot Eng 37(1):183–190 (**in Chinese**)
22. Al-Jeznawi D, Jais I, Albusoda B (2022) (2022) A soil–pile response under coupled static dynamic loadings in terms of kinematic interaction. J Civ Environ Eng 18(1):96–103. https://doi.org/10.2478/cee-2022-0010
23. Al-Tameemi S (2018) Experimental and numerical study on the effect of liquefaction potential of piles in sandy layers of soil under earthquake loading. Ph.D. Thesis, Civil Engineering Department, University of Al-Nahrain
24. Maymand P, Reimer M, Seed R (2000) Large scale shaking table tests of seismic soil-pile interaction in soft clay. In: Proceedings of 12th world conference on earthquake engineering, New Zealand, vol 5, p 915
25. Ternet O (1999) Reconstitution et caractérisation des massifs de sable: application aux essais en centrifugeuse et en chambre de calibration. Doctoral dissertation, Caen
26. Garnier J (2002) Size effect in shear interfaces. In: Proceedings workshop on constitutive and centrifuge modelling: two extremes, Monte Verita, Switzerland, pp 335–346
27. Nateghi A (2015) Numerical modelling of sand behavior under cyclic simple shear tests in a special liquefaction box. Doctoral dissertation, MSc Thesis, Istanbul Technical University, Istanbul, Turkey.
28. Al-Salakh A, Albusoda B (2020) (2020) Experimental and theoretical determination of settlement of shallow footing on liquefiable soil. J Eng 26(9):64–155
29. Ishihara K (1985) Stability of natural deposits during earthquakes. In: Procs of the Elevh Int Conf Soil Mechs and Found Eng, pp 321–376, San Francisco, 12–16 August 1985. Publication of: Balkema (AA)